Supporting Information for

Oxygen Vacancies Mediated and Enhanced Metal-P Bonds for Stabilizing Reconstruction toward Alkaline Freshwater and Seawater Electrolysis

Lei Jin, Hui Xu*, Kun Wang, Yang Liu, Xingyue Qian, Guangyu He*, Haiqun Chen*

Key Laboratory of Advanced Catalytic Materials and Technology, Advanced Catalysis and Green Manufacturing Collaborative Innovation Center, Changzhou University, Changzhou, Jiangsu Province 213164, China

Corresponding authors: xuhui006@cczu.edu.cn (H. Xu), hegy@cczu.edu.cn (G. He); chenhq@cczu.edu.cn (H. Chen)

1. Material characterizations

The crystal phases and structures of the as-prepared samples were characterized by powder X-ray diffraction (XRD) with Bruker D8 Advance diffractometer (Cu Ka radiation, $\lambda = 0.15418$ nm) in the 2θ range of 20-80° at a scanning rate of 0.05° s^{-1}. The microstructures of the products were observed by transmission electron microscopy (TEM, JEM-2100F) and field-emission scanning electron microscopy (FESEM, Zeiss Supra 55) that equipped with element mappings. The morphologies of the materials were characterized by scanning electron microscopy (SEM, Zeiss Sigma 300 Cold Field scanning electron microscope). X-ray photoelectron spectroscopy (XPS, PHI-5000C ESCA, PerkinElmer, USA) was employed to obtain elemental information of prepared catalysts on a VG ESCALAB MKII using Al Ka radiation. The Fourier transform infrared spectrometer (FT-IR, Nicolet iS5) was recorded to detect the functional groups of samples in the range of 200-2000 cm^{-1}. The electron paramagnetic resonance (EPR) spectra were recorded on a Bruker EPR ELEXSYS 500 spectrometer. The absorbance data of spectrophotometer were measured on UV-2700 spectrophotometer.

2. Electrochemical measurements

All the electrochemical measurements were tested using a CHI760E electrochemical workstation with a standard three electrode cell. The reference and counter electrodes were Hg/HgO and graphite rod, respectively. A glassy carbon electrode (GCE. 5 mm inner diameter, 0.196 cm^2 area) that modified with catalyst ink is used as the working electrode. The homogeneous catalyst ink was made by ultrasonically dispersing a mixture containing 2 mg of catalyst, 20 μL Nafion (5 wt%),

360 μL ethanol and 120 μL H_2O. Then, 13 μL of the catalyst ink was dropped on the surface of GCE with an approximate mass loading of 265.0 μg·cm^{-2}. All potentials were measured against Hg/HgO and converted to reversible hydrogen electrode (RHE) by Nernst equation: $E_{vs\ RHE} = E_{vs\ Hg/HgO} + 0.0591 \cdot pH + 0.098$. The overpotential (η) was calculated through the formula: $\eta = E_{RHE} - 1.23$ V. Cyclic Voltammograms (CV) were measured at a scan rate of 5 mV·s^{-1}. Electrochemical impedance spectroscopy was tested over the frequency range of 10^6 to 10^{-2} Hz with an AC signal amplitude of 5 mV. The double-layer capacitance (C_{dl}) was evaluated by cyclic voltammetry (CV) curves performed at the non-faraday reaction regions with an interval of 20 mV·s^{-1} over the scanning range of 20 ~ 120 mV·s^{-1}. Specifically, the electrochemical active area ECSA is calculated by the formula ECSA = C_{dl}/C_s, where C_{dl} is the electric double layer capacitance and C_s is the characteristic capacitance of the material (usually 0.04 mF cm^{-2}). The turnover frequency (TOF) values were calculated from the following equation: TOF (s^{-1}) = (j × A)/ (k × F × n). Here, k is the number of electron transfer (the factors of HER and OER are respectively 2 and 4), j is the current density at a given overpotential, A is the geometric surface area of the electrode, F is the Faraday constant (96485.3 C mol^{-1}), n is the number of active sites (mol). The number of voltammetric charges is gained by CV curves from -0.6 ~ 0 V and 0 ~ 0.6 V *vs*. RHE for OER and HER in phosphate buffer solution (pH = 7) with a scan rate of 50 mV s^{-1} respectively, and the following equation is n (mol) = Q/2F (the surface charge Q is proportional to the number of active sites). The long-term stability of the catalyst was conducted by chronoamperometry (CA) and chronopotentiometry (CP). All the data of

electrochemistry were presented without any iR correction.

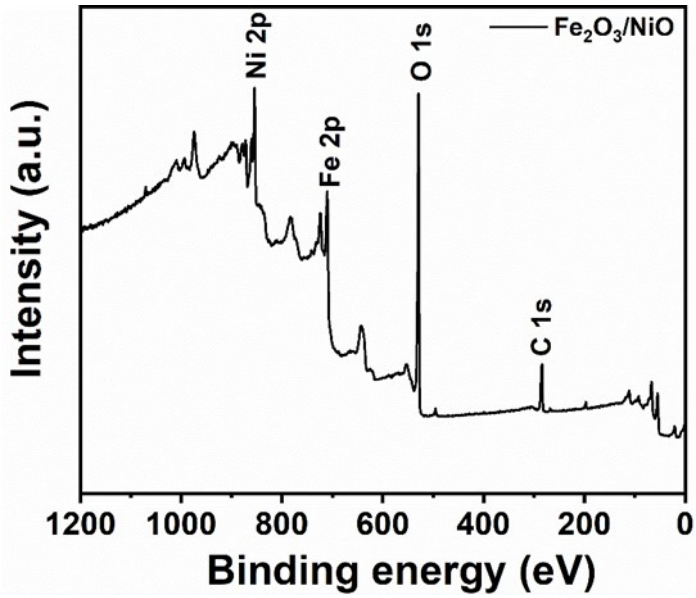

Fig. S1 XPS full spectrum of the NiO/Fe_2O_3.

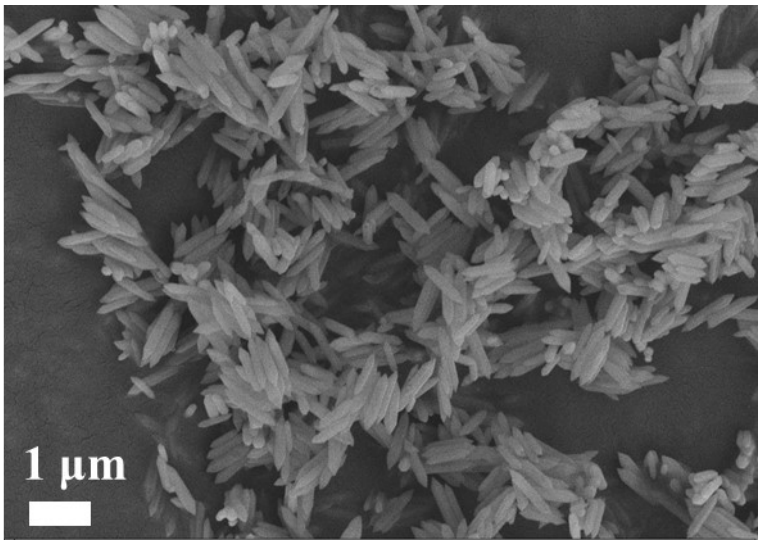

Fig. S2 SEM image of the MIL-NiFe.

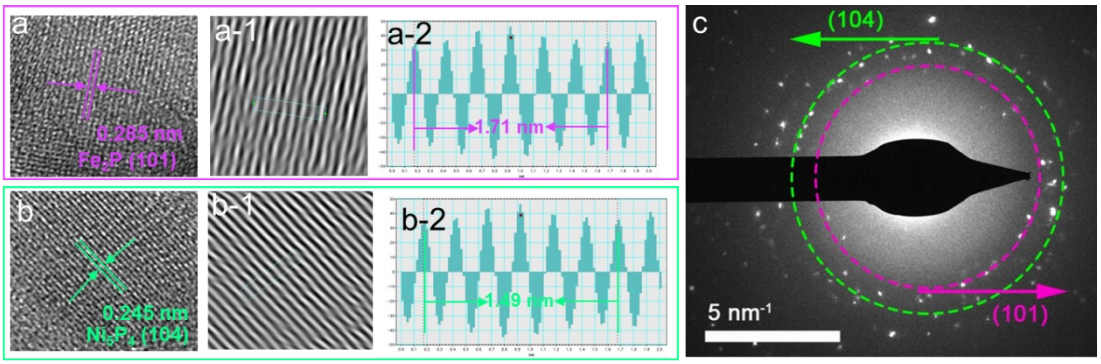

Fig.S3 (a, b) High-resolution TEM of Fe_2P/Ni_5P_4, integrated pixel intensities (a-2 and b-2) of Fe_2P and Ni_5P_4 (taken from the green dotted rectangle in (a-1) and (b-1)). (c) SAED pattern of Fe_2P/Ni_5P_4.

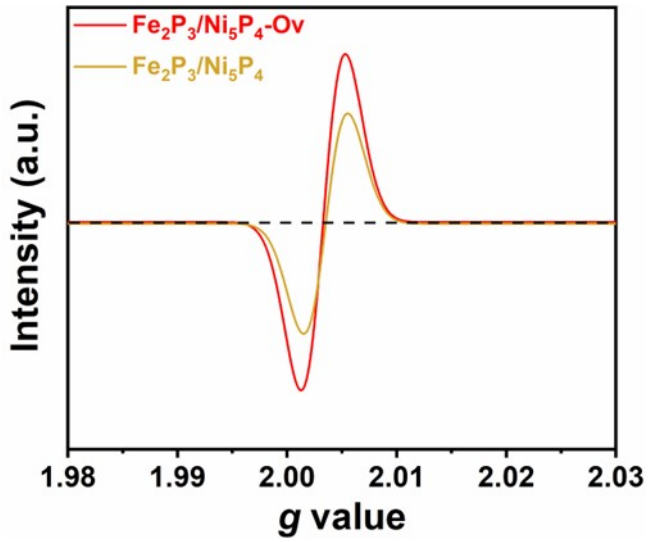

Fig. S4 EPR spectra of Fe_2P/Ni_5P_4-Ov and Fe_2P/Ni_5P_4.

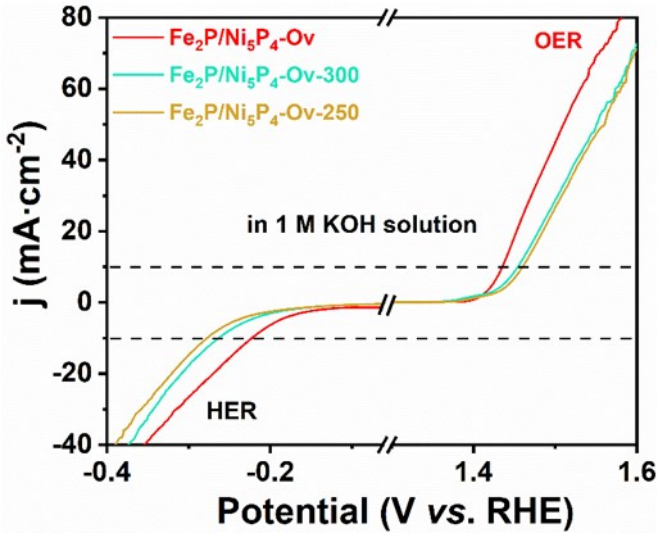

Fig.S5 Electrocatalytic OER and HER performance of Fe_2P/Ni_5P_4-Ov, Fe_2P/Ni_5P_4-Ov-300 and Fe_2P/Ni_5P_4-Ov-250 in 1 M KOH solution.

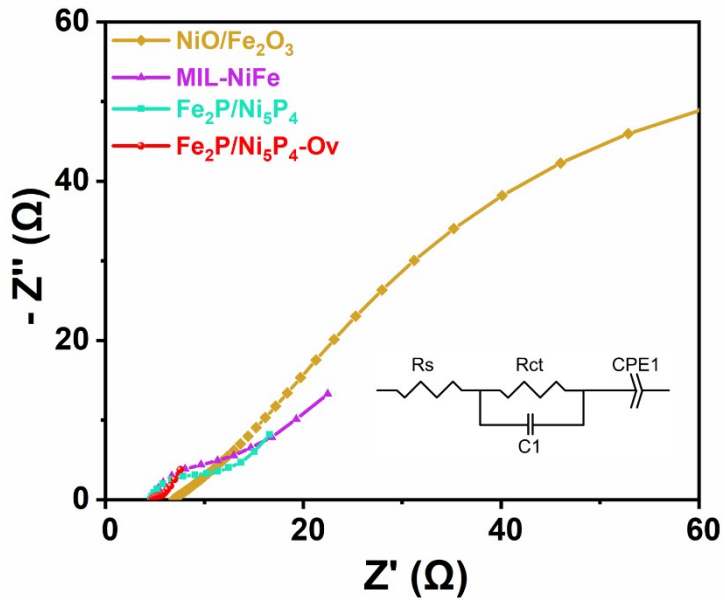

Fig. S6 EIS curves of Fe_2P/Ni_5P_4-Ov with other samples for OER in 1.0 M KOH solution.

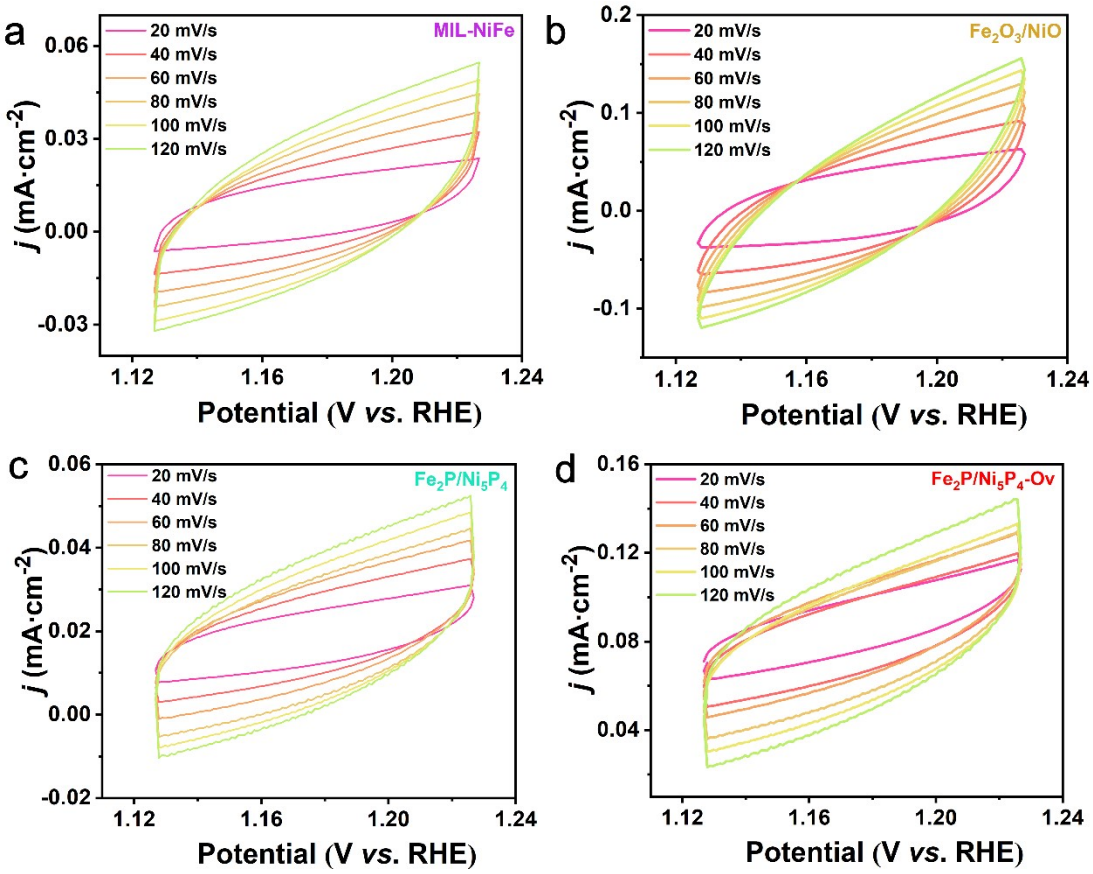

Fig. S7 CV curves of different electrocatalysts with different scanning rates for OER in 1.0 M KOH solution.

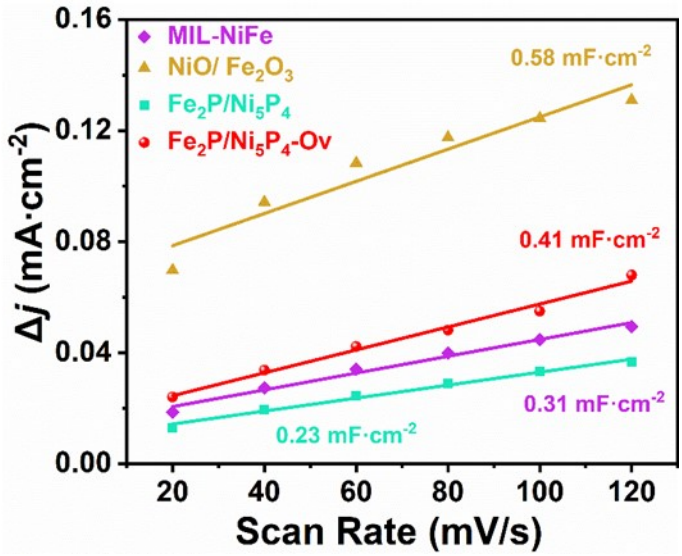

Fig. S8 C_{dl} values of different catalysts for OER in 1.0 M KOH solution.

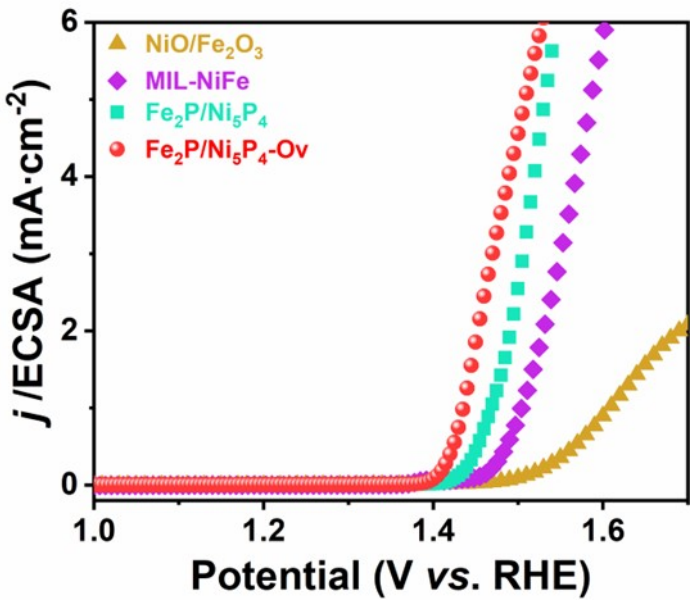

Fig. S9 LSV curves normalized to the ECSA.

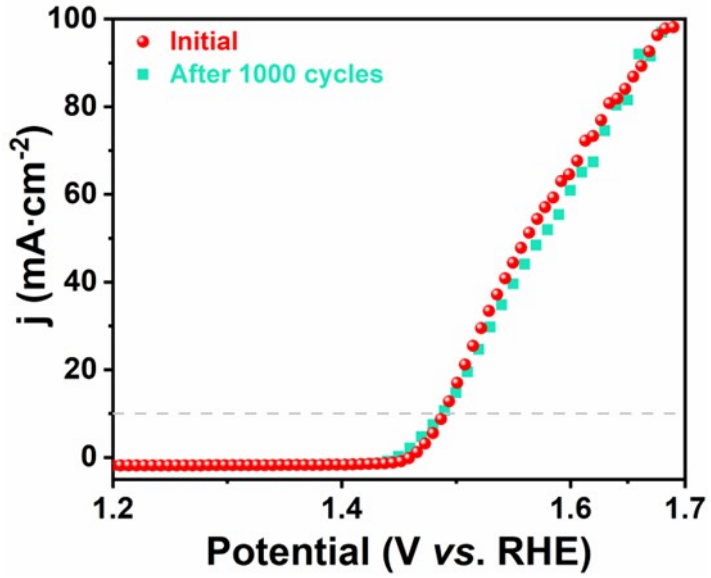

Fig. S10 LSV curves of Fe_2P/Ni_5P_4-Ov before and after 1000 potential CV cycles for OER.

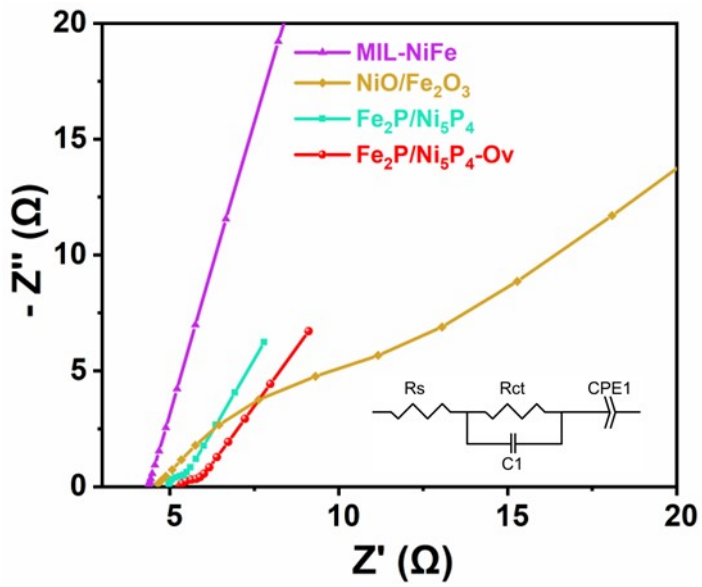

Fig. S11 EIS curves of Fe_2P/Ni_5P_4-Ov with other samples for HER in 1.0 M KOH solution.

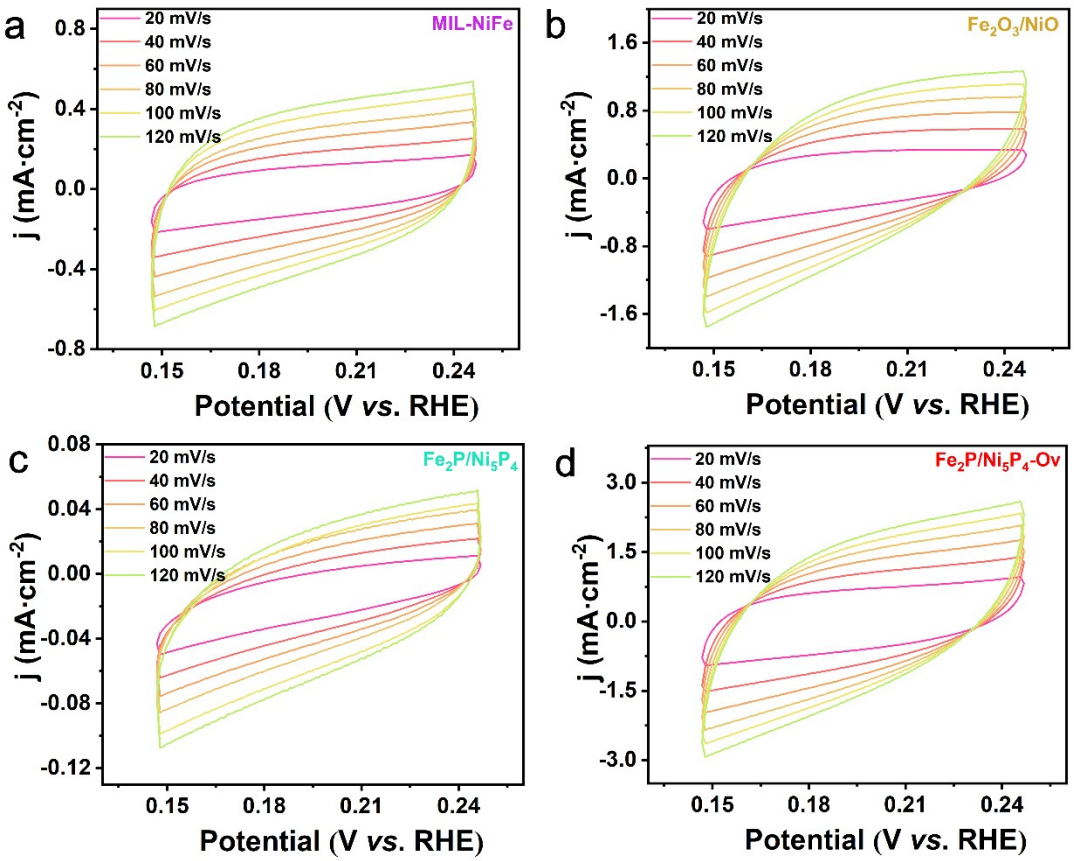

Fig. S12 CV curves of different electrocatalysts with different scanning rates for HER in 1.0 M KOH solution.

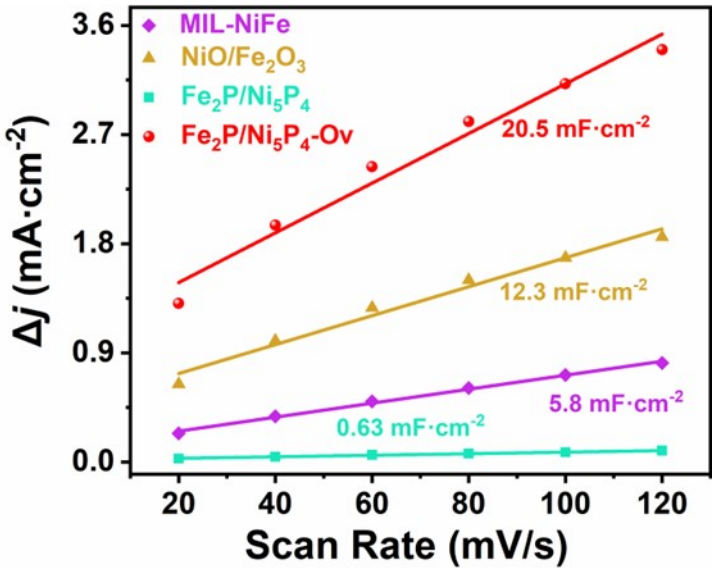

Fig. S13 C_{dl} values of different catalysts for HER in 1.0 M KOH solution.

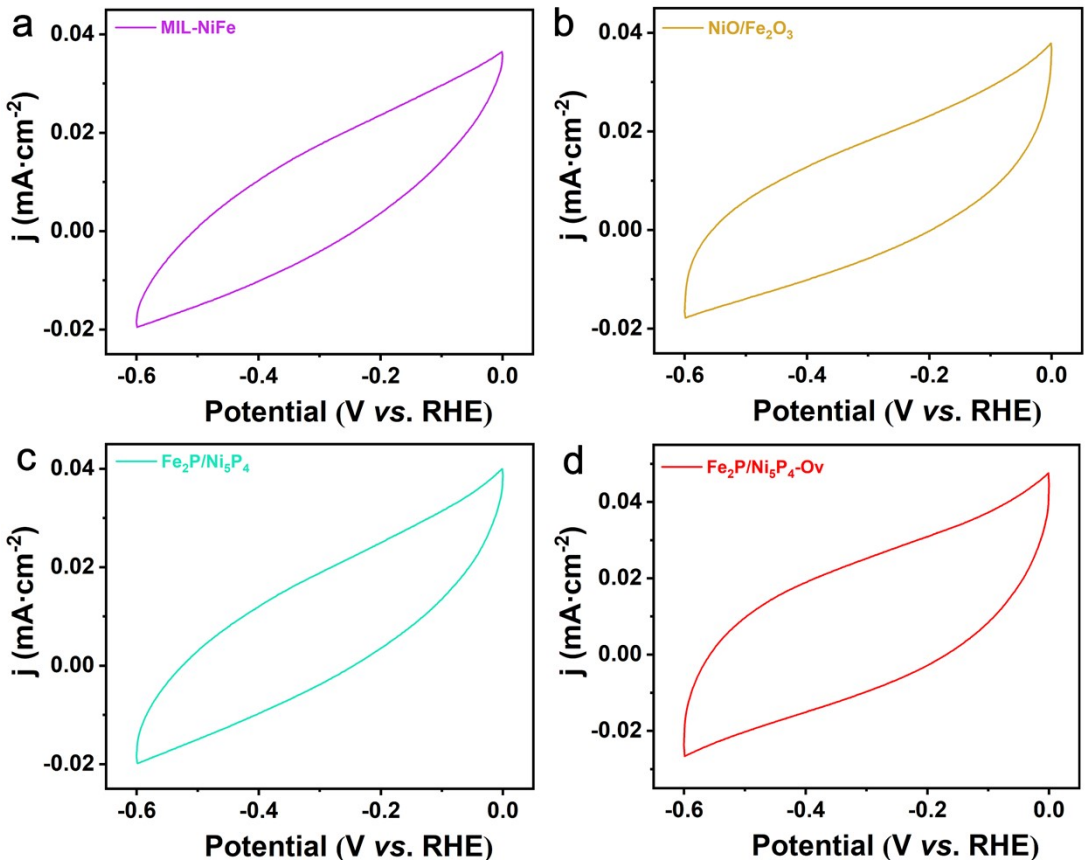

Fig. S14 CV curves from -0.6 to 0 V *vs.* RHE for OER in 1.0 M PBS (pH = 7) at 50 mV s^{-1}.

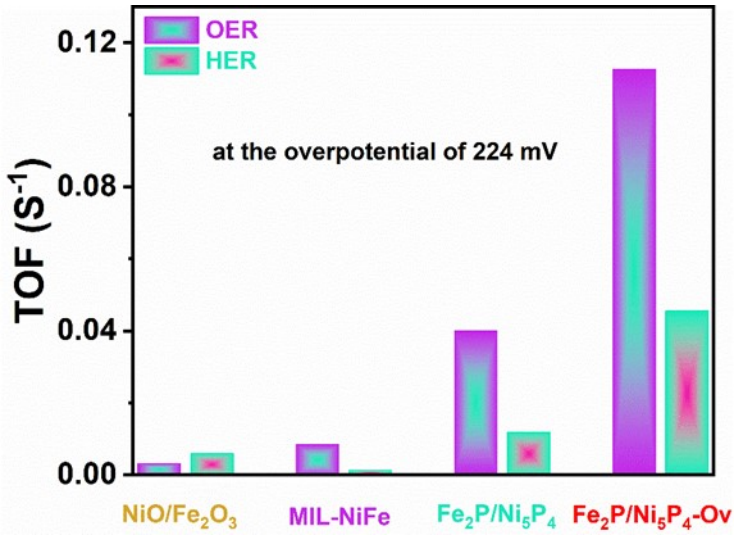

Fig. S15 TOF values of different catalysts for OER and HER in 1.0 M KOH + freshwater solution.

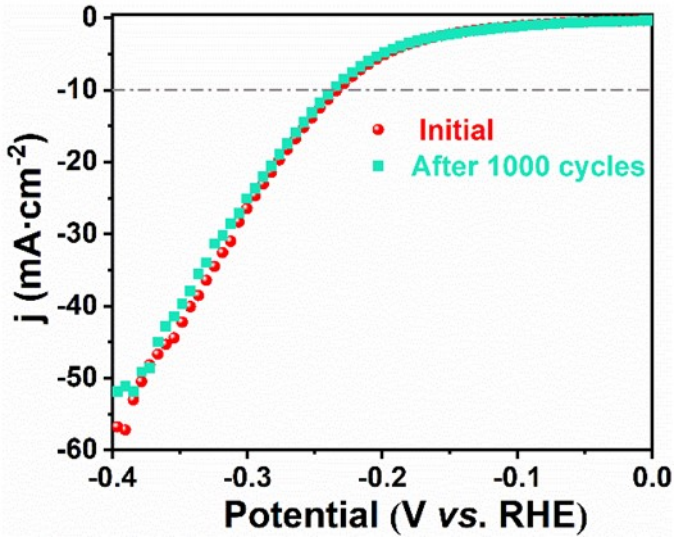

Fig. S16 LSV curves of Fe_2P/Ni_5P_4-Ov before and after 1000 potential CV cycles for HER.

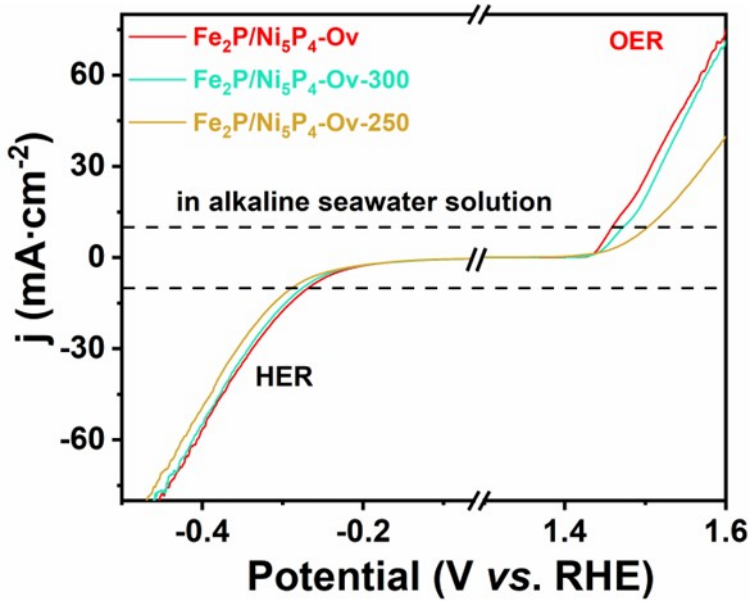

Fig.S17 Electrocatalytic OER and HER performance of Fe_2P/Ni_5P_4-Ov, Fe_2P/Ni_5P_4-Ov-300 and Fe_2P/Ni_5P_4-Ov-250 in alkaline seawater solution.

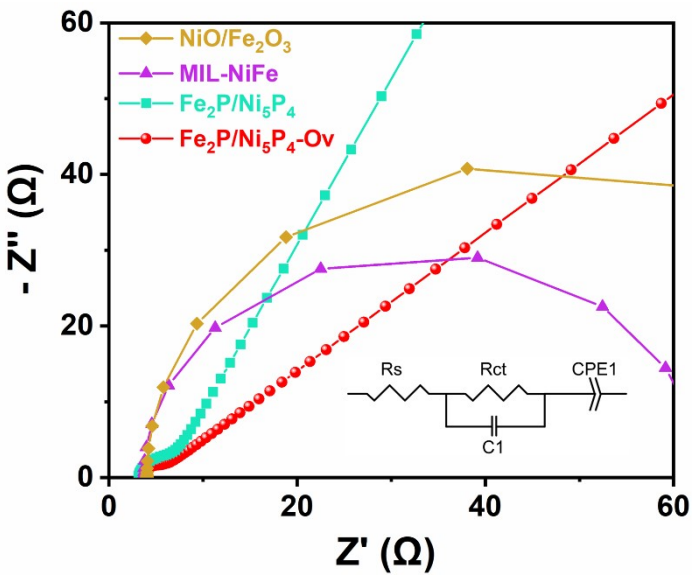

Fig. S18 EIS curves of Fe_2P/Ni_5P_4-Ov with other samples for OER in 1.0 M KOH + seawater solution.

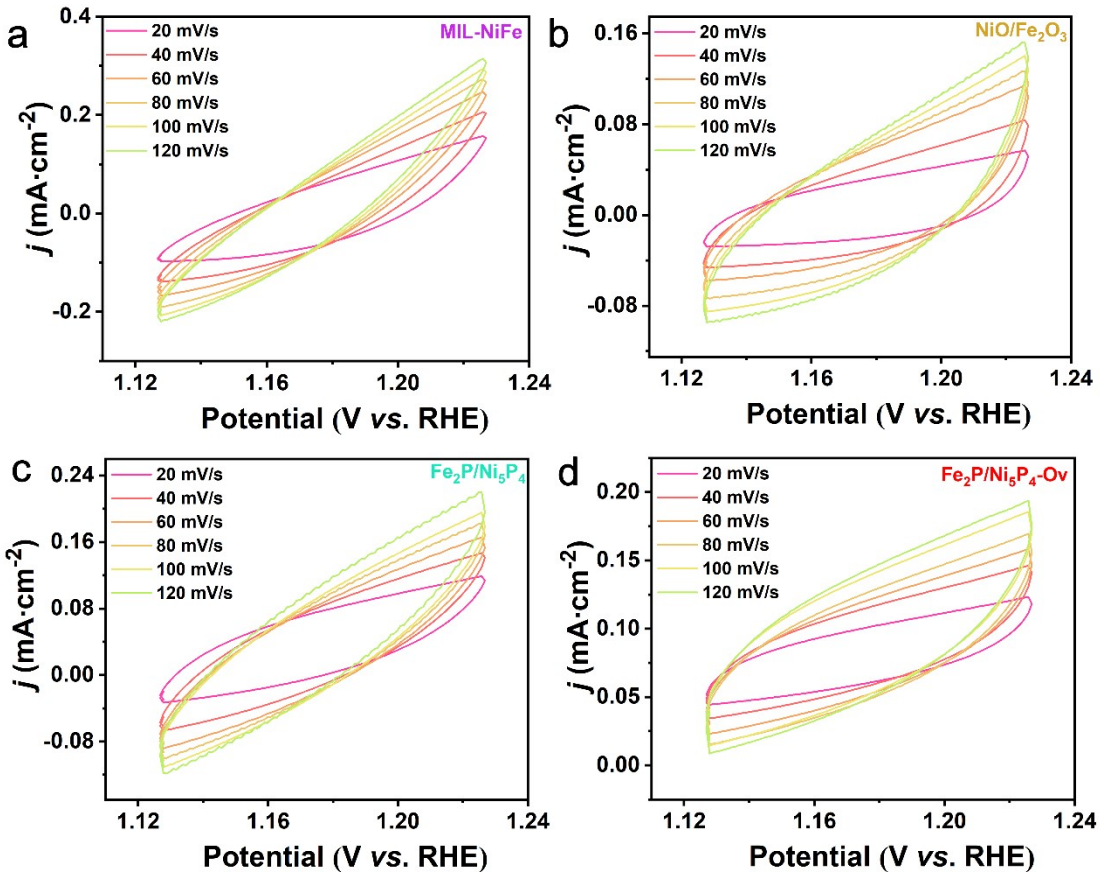

Fig. S19 CV curves of different electrocatalysts with different scanning rates for OER in 1.0 M KOH + seawater solution.

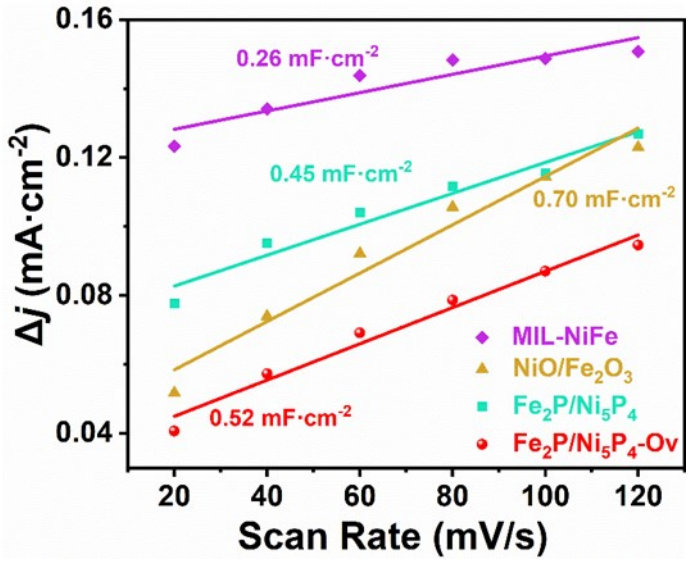

Fig. S20 C_{dl} values of different catalysts for OER in 1.0 M KOH + seawater solution.

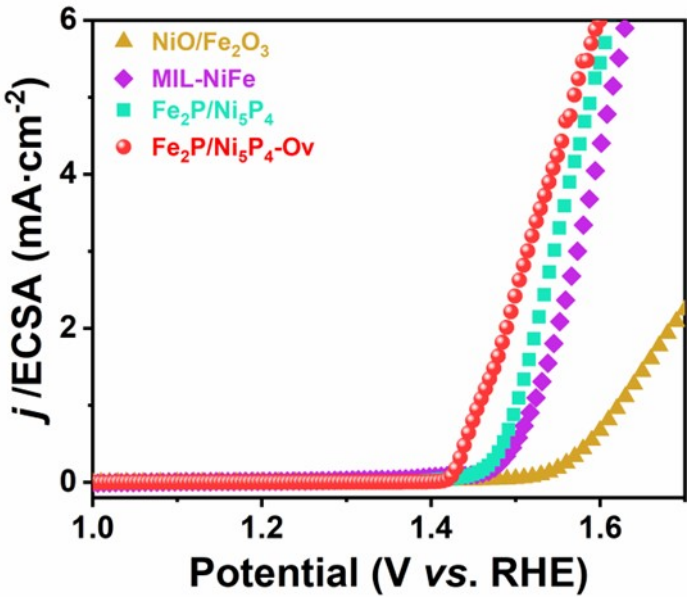

Fig. S21 LSV curves normalized to the ECSA.

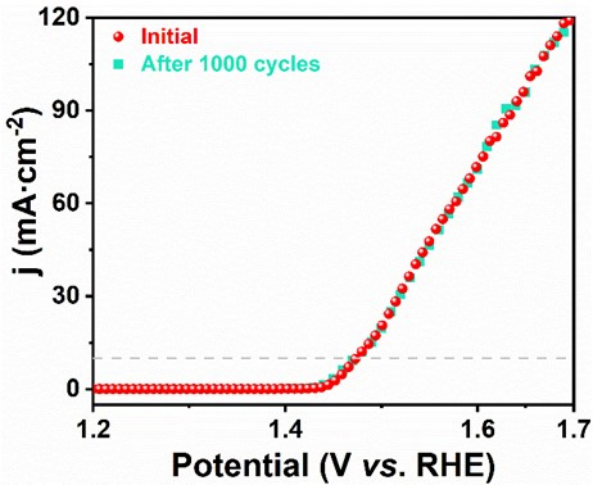

Fig. S22 LSV curves of Fe_2P/Ni_5P_4-Ov before and after 1000 potential CV cycles for OER.

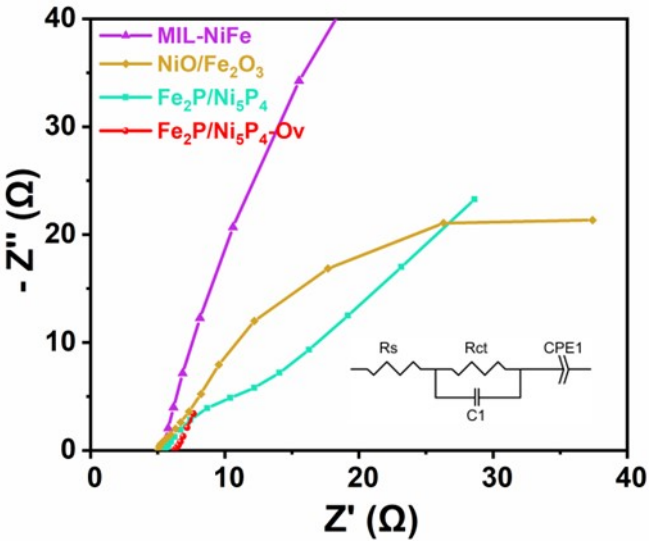

Fig. S23 EIS curves of Fe_2P/Ni_5P_4-Ov with other samples for HER in 1.0 M KOH+ seawater solution.

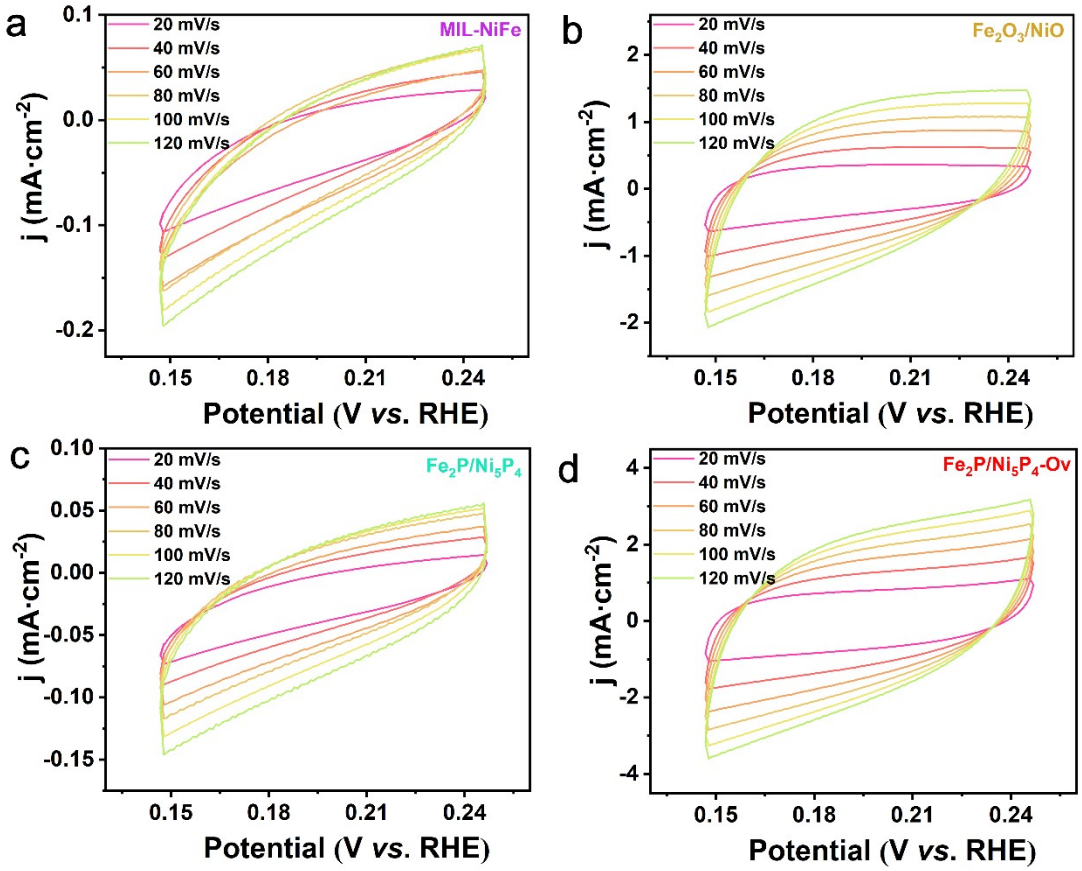

Fig. S24 CV curves of different electrocatalysts with different scanning rates for HER in 1.0 M KOH + seawater solution.

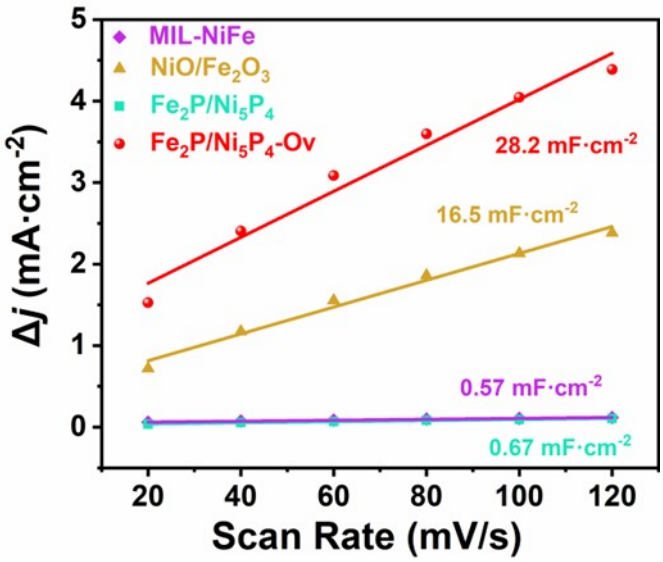

Fig. S25 C_{dl} values of different catalysts for HER in 1.0 M KOH + seawater solution.

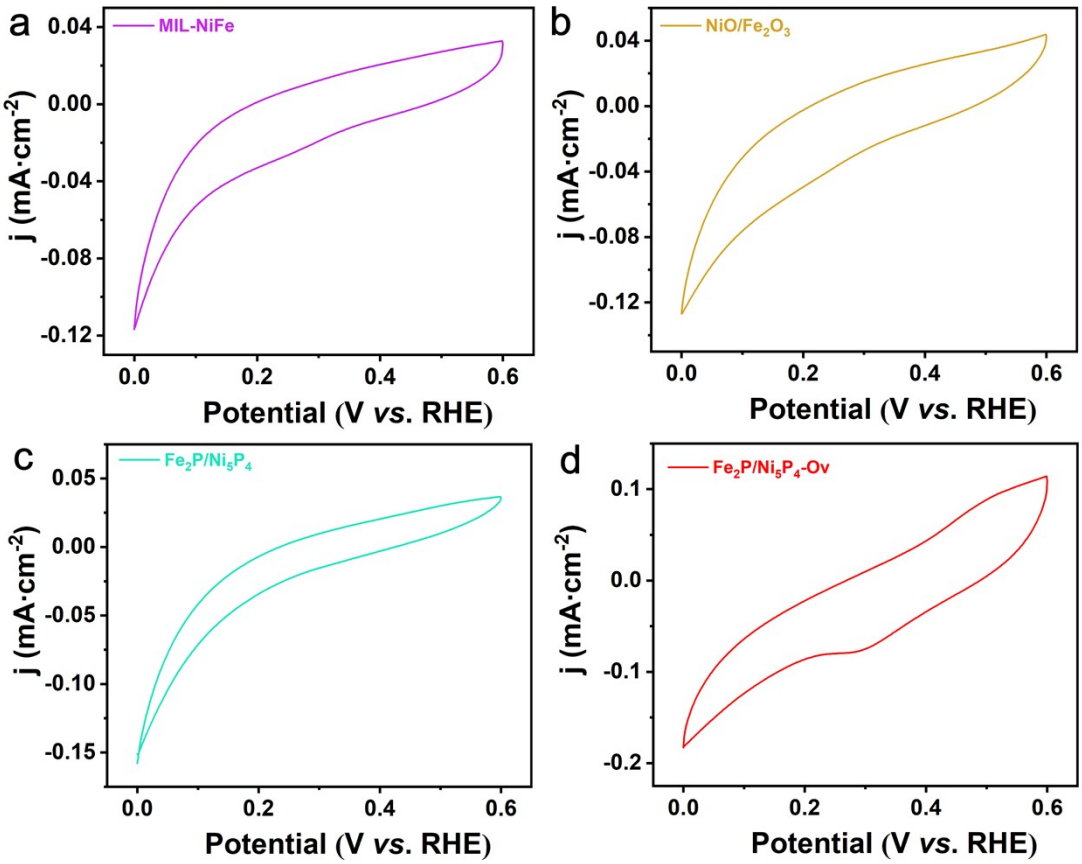

Fig. S26 CV curves from 0 to 0.6 V *vs.* RHE for HER in 1.0 M PBS (pH = 7) at 50 mV s^{-1}.

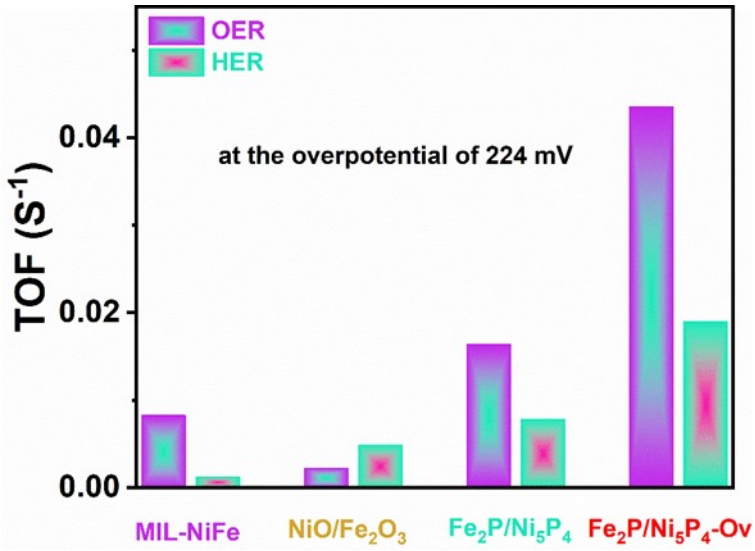

Fig. S27 TOF values of different catalysts for OER and HER in 1.0 M KOH + seawater solution.

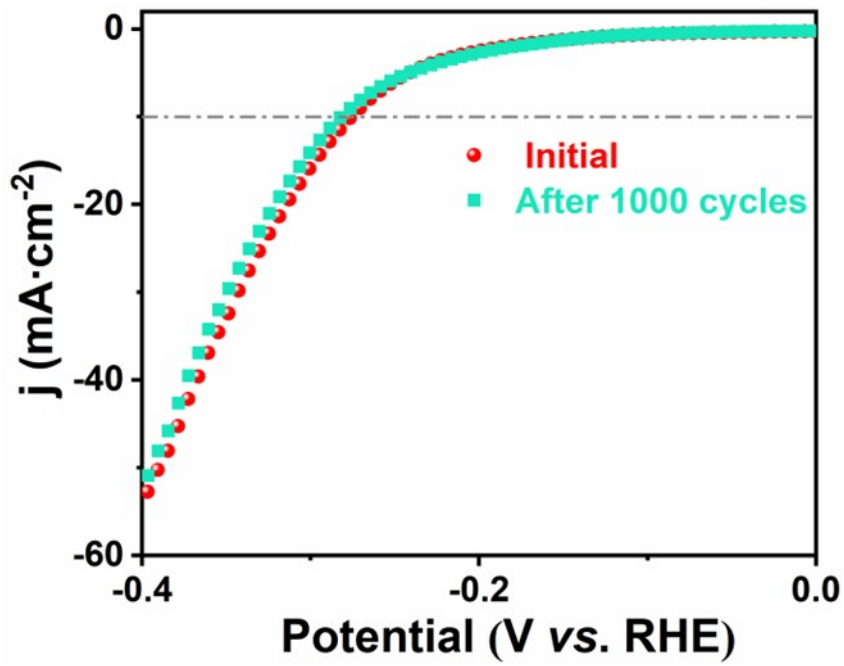

Fig. S28 LSV curves of Fe_2P/Ni_5P_4-Ov before and after 1000 potential CV cycles for HER.

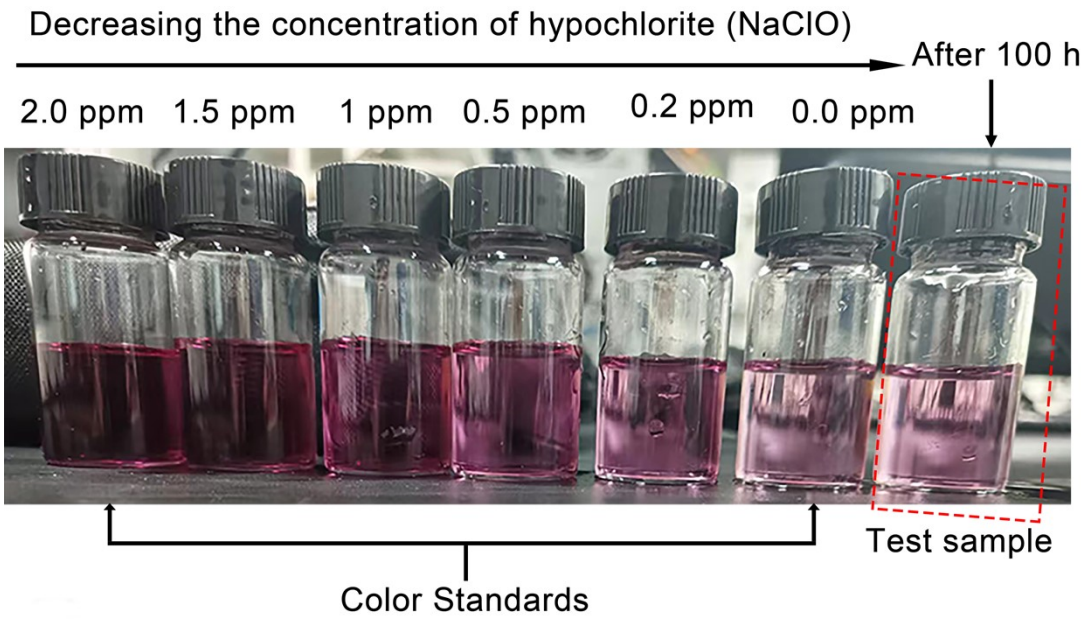

Fig. S29 Hypochlorite detection result with different NaClO contents and the electrolyte after 100 h electrolysis for Fe_2P/Ni_5P_4-Ov at a constant current density of 10 mA cm^{-2} in 1 M KOH + seawater.

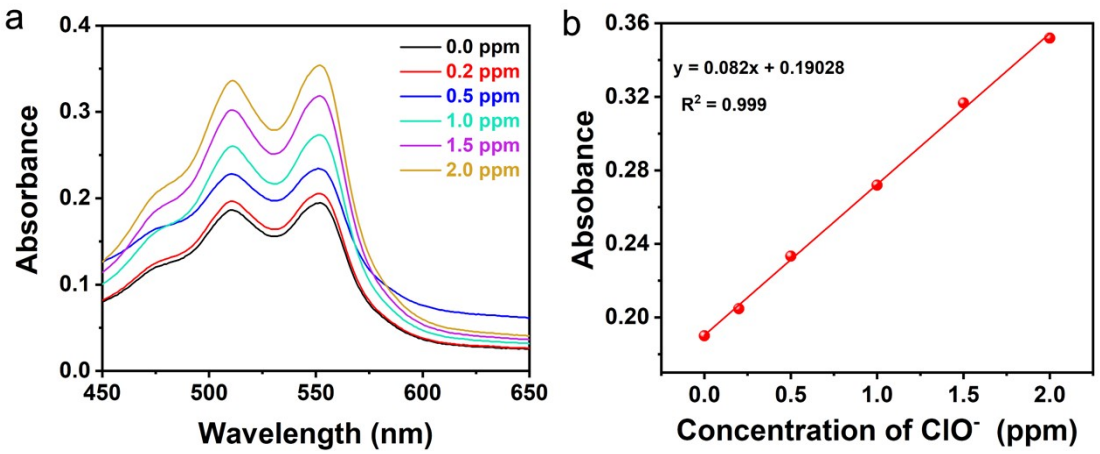

Fig. S30 (a) UV-Vis absorption spectra of ClO^- with different concentrations. (b) Calibration curve used for calculating ClO^- concentrations of the electrolyte.

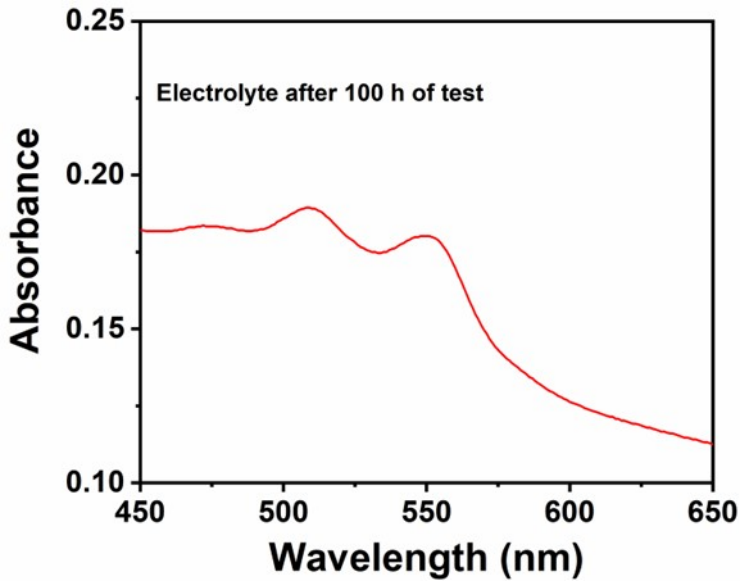

Fig. S31 UV/Vis absorption spectrum of the electrolyte after 100 h electrolysis for Fe_2P/Ni_5P_4-Ov at a constant current density of 10 mA cm^{-2} in 1 M KOH + seawater.

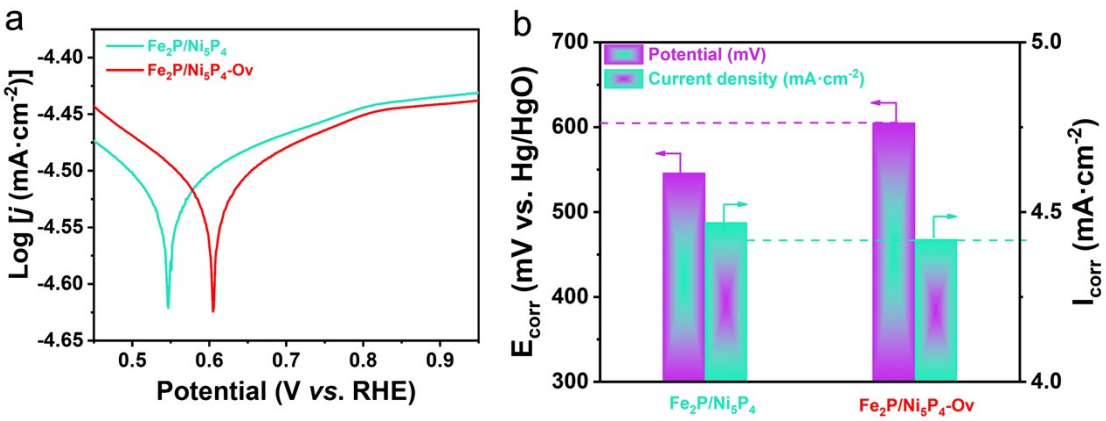

Fig. S32 (a) Polarization curves for corresponding electrodes after OCP test. (b) comparison of Ecorr and Icorr on Fe_2P/Ni_5P_4 and Fe_2P/Ni_5P_4-Ov.

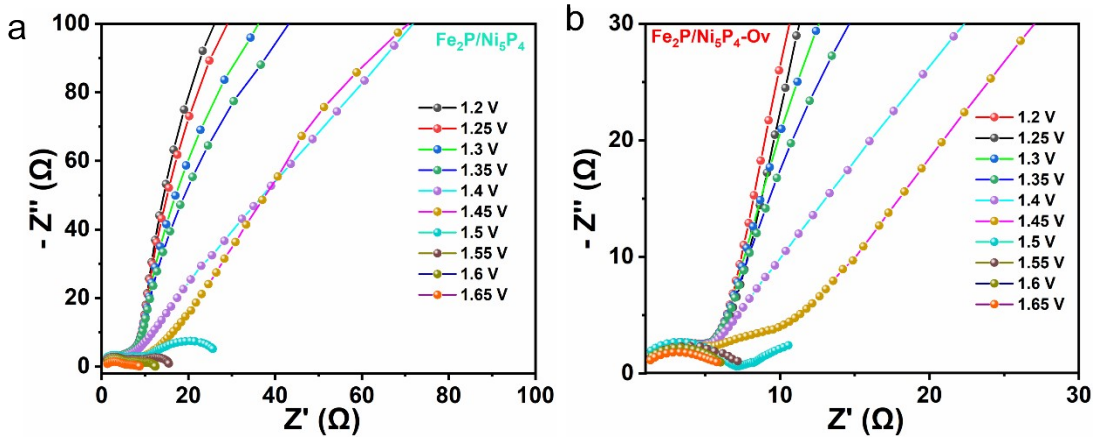

Fig. S33 Nyquist plots for (a) Fe_2P/Ni_5P_4 and (b) Fe_2P/Ni_5P_4-Ov at different applied potentials *vs* RHE in 1 M KOH solution.

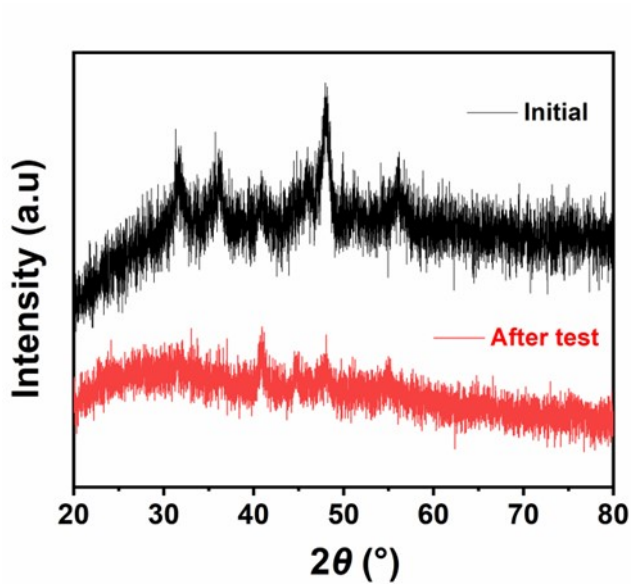

Fig. S34 XRD pattern of the Fe_2P/Ni_5P_4-Ov catalyst before and after the OER test.

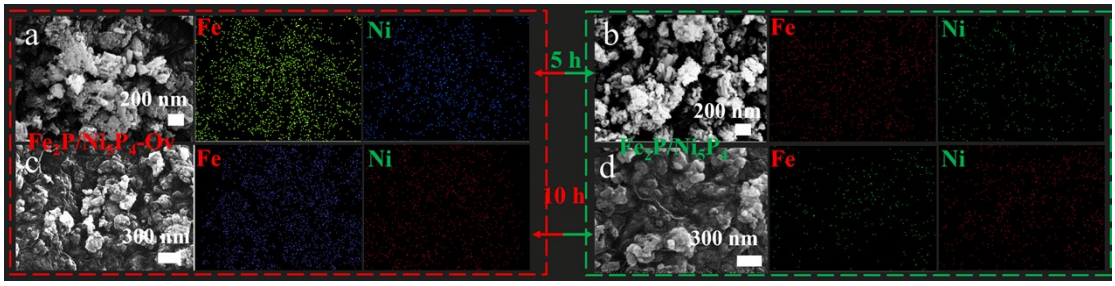

Fig. S35 (a, b) EDX elemental mappings of Fe_2P/Ni_5P_4-Ov and Fe_2P/Ni_5P_4 catalysts that cycled for 5 h, respectively. (c, d) EDX elemental mappings of Fe_2P/Ni_5P_4-Ov and Fe_2P/Ni_5P_4 catalysts that cycled for 10 h, respectively

Table S1. Comparison of OER performance with other electrocatalysts 1.0 M KOH solution.

Catalysts	Overpotential (mV)	Current density (mA cm^{-2})	Ref
Fe_2P/Ni_5P_4-Ov	**205**	**10**	**This work**
CoP_2/NC-1	290	10	1
Ir@Zr-CoP	292	10	2
Ru-MoCoP	240	10	3
Ni_2P/Ni_5P_4	286	10	4
CoP@CNF	300	10	5
CoP/NiCoP	310.7	10	6
CoP/Mo_2CT_x	312	10	7
Ru-RuPxCoxP	338	10	8
Fe-Co-P	340	10	9
Mn-CoP-2	344	10	10
V-CoP	420	10	11

Table S2. List of resistance values calculated from electrical impedance spectra of NiO/Fe_2O_3, MIL-NiFe, Fe_2P/Ni_5P_4 and Fe_2P/Ni_5P_4-Ov for OER in 1.0 M KOH solution. (R_s: Electrolyte resistance; R_{ct}: Charge transfer resistance).

Materials	**R_s (ohm)**	**R_{ct} (ohm)**
Fe_2P/Ni_5P_4-Ov	4.762	1.02
Fe_2P/Ni_5P_4	4.824	6.4
MIL-NiFe	1.23	15.7
NiO/Fe_2O_3	5.0	48.6

Table S3. List of resistance values calculated from electrical impedance spectra of NiO/Fe_2O_3, MIL-NiFe, Fe_2P/Ni_5P_4 and Fe_2P/Ni_5P_4-Ov for HER in 1.0 M KOH solution. (R_s: Electrolyte resistance; R_{ct}: Charge transfer resistance).

Materials	**R_s (ohm)**	**R_{ct} (ohm)**
Fe_2P/Ni_5P_4-Ov	4.656	0.37
Fe_2P/Ni_5P_4	4.683	0.46
MIL-NiFe	7.52	94.5
NiO/Fe_2O_3	4.9	3.1

Table S4. List of resistance values calculated from electrical impedance spectra of NiO/Fe_2O_3, MIL-NiFe, Fe_2P/Ni_5P_4 and Fe_2P/Ni_5P_4-Ov for OER in alkaline seawater solution. (R_s: Electrolyte resistance; R_{ct}: Charge transfer resistance).

Materials	**R_s (ohm)**	**R_{ct} (ohm)**
Fe_2P/Ni_5P_4-Ov	3.109	1.5
Fe_2P/Ni_5P_4	3.129	2.9
MIL-NiFe	3.859	36.2
NiO/Fe_2O_3	3.71	46.7

Table S5. List of resistance values calculated from electrical impedance spectra of NiO/Fe_2O_3, MIL-NiFe, Fe_2P/Ni_5P_4 and Fe_2P/Ni_5P_4-Ov for HER in alkaline seawater solution. (R_s: Electrolyte resistance; R_{ct}: Charge transfer resistance).

Materials	**R_s (ohm)**	**R_{ct} (ohm)**
Fe_2P/Ni_5P_4-Ov	4.461	0.19
Fe_2P/Ni_5P_4	4.48	3.2
MIL-NiFe	4.79	107.3
NiO/Fe_2O_3	4.6	26.1

Table S6 Comparison of OER performance in alkaline seawater solution for Fe_2P/Ni_5P_4-Ov with some representative non-precious metal catalysts reported.

Catalysts	Overpotential (mV)	Currentdensity (mA cm^{-2})	Tafels lope (mV/dec)	Ref.
Fe_2P/Ni_5P_4-Ov	**229**	**10**	**56.3**	**This work**
Fe_2P-NiCoP	258	10	49	12
FCNP@CQs	268	10	45.2	13
$CoSe_2$-NCF	245	10	93	14
Er-MoO_2	312	10	99	15
ER-SNCF-20s	278	10	57	16
Fe_2P-NiCoP	245	10	82.5	17
NiMoSe@CC	360	10	—	18
$Co_2P/CoMoP_2$	268	10	81	19

References

1. Chen, Y.; Yang, Z.; Wang, J.; Yang, Y.; He, X.; Wang, Y.; Chen, J.; Guo, Y.; Wang, X.; Wang, S., *Nano Res.,* 2023, **17,** 1-9.

2. Ngo, Q. P.; Nguyen, T. T.; Le, Q. T. T.; Lee, J. H.; Kim, N. H., *Adv. Energy Mater.,* 2023, **13** (44), 2301841.

3. Bi, M.; Zhang, Y.; Jiang, X.; Sun, J.; Wang, X.; Zhu, J.; Fu, Y., *Adv. Energy Mater.,* 2024, **34** (2), 2309330.

4. Lyu, C.; Cao, C.; Cheng, J.; Yang, Y.; Wu, K.; Wu, J.; Lau, W.-M.; Qian, P.; Wang, N.; Zheng, J., Chem. Eng. J., 2023, **464**, 142538.

5. Ren, A.; Yu, B.; Huang, M.; Liu, Z., *Int. J. Hydrogen Energy,* 2024, **51**, 490-502.

6. Fu, X.; Zhang, Z.; Zheng, Y.; Lu, J.; Cheng, S.; Su, J.; Wei, H.; Gao, Y., *J. Colloid Interf. Sci.,* 2024, **653**, 1272-1282.

7. Liu, S.; Lin, Z.; Wan, R.; Liu, Y.; Liu, Z.; Zhang, S.; Zhang, X.; Tang, Z.; Lu, X.; Tian, Y., *J. Mater. Chem. A,* 2021, **9** (37), 21259-21269.

8. Wang, L.; Zhou, Q.; Pu, Z.; Zhang, Q.; Mu, X.; Jing, H.; Liu, S.; Chen, C.; Mu, S., *Nano Energy,* 2018, **53,** 270-276.

9. Liu, K.; Zhang, C.; Sun, Y.; Zhang, G.; Shen, X.; Zou, F.; Zhang, H.; Wu, Z.; Wegener, E. C.; Taubert, C. J., *ACS Nano,* 2018, **12** (1), 158-167.

10. Liu, Y.; Ran, N.; Ge, R.; Liu, J.; Li, W.; Chen, Y.; Feng, L.;Che, R., *Chem. Eng. J.,*2021, **425**, 131642.

11. Zhang, R.; Wei, Z.; Ye, G.; Chen, G.; Miao, J.; Zhou, X.; Zhu, X.; Cao, X.; Sun, X., Adv. Energy Mater., 2021**, 11** (38), 2101758.

12. Xiao, M.; Zhang, C.; Wang, P.; Zeng, W.; Zhu, J.; Li, Y.; Peng, W.; Liu, Q.; Xu, H.;Zhao, Y., Mater. *Today Phys.*, 2022**, 24**, 100684.

13. Lv, S.; Deng, Y.; Liu, Q.; Fu, Z.; Liu, X.; Wang, M.; Xiao, Z.; Li, B.; Wang, L., *Appl. Catal. B: Environ. Energy,* 2023, **326**, 122403.

14. Chen, H.; Zhang, S.; Liu, Q.; Yu, P.; Luo, J.; Hu, G.;Liu, X., *Inorg. Chem. Commun.,* 2022, **146**, 110170.

15. Yang, T.; Lv, H.; Quan, Q.; Li, X.; Lu, H.; Cui, X.; Liu, G.;Jiang, L., *Appl. Surf. Sci.,* 2023, **615**, 156360.

16. Hu, R.; Zhao, M.; Miao, H.; Liu, F.; Zou, J.; Zhang, C.; Wang, Q.; Tian, Z.; Zhang, Q.;Yuan, J., *Nanoscale,* 2022, **14** (28), 10118-10124.

17. Jin, L.; Xu, H.; Wang, K.; Yang, L.; Liu, Y.; Qian, X.; He, G.;Chen, H., Appl. Surf. Sci., 2024, **657,** 159777.

18. Saquib, M.; Arora, P.;Bhosale, A. C., *Fuel,* 2024, **365**, 131251.

19. Sun, B.; Li, C.; Yang, J.; Bai, H.;Meng, X., *Inorg. Chem. Front.,* 2024, **11**, 1978-1992.